Magnetic anisotropy and weak ferromagnetism of single-crystal $TbNi_2B_2C$

B. K. Cho, P. C. Canfield, and D. C. Johnston
Ames Laboratory and Department of Physics and Astronomy, Iowa State University, Ames, Iowa 50011
(Received 13 September 1995)

The anisotropic magnetization $M(T)$ of single-crystal $TbNi_2B_2C$ is reported as a function of applied magnetic field (**H**) for temperatures T from 2 to 300 K and with **H** parallel and perpendicular to the c axis ($\mathbf{H}\|\mathbf{c}$ and $\mathbf{H}\perp\mathbf{c}$). In low field ($H\leqslant 100$ G) $TbNi_2B_2C$ orders antiferromagnetically at Néel temperature $T_N=(14.9\pm 0.1)$ K. Weak ferromagnetic (WF) behavior is found for $T\leqslant 8$ K and $H\leqslant 10$ kG. Both phase transitions are also detected in zero-field in-plane resistivity $\rho_{ab}(T)$ measurements. In contrast, previous low-field $M(T,H)$ data showed antiferromagnetic ground states for (Gd,Dy,Ho,Er,Tm)Ni_2B_2C crystals. The origin of the WF ordering, given the point symmetry ($4/mmm$) of the Tb^{+3} ions, is addressed together with the observed in-plane anisotropy in the high-field magnetization. Possible reasons for the absence of superconductivity above 2 K in $TbNi_2B_2C$ are also discussed. Finally, a partial H-T magnetic phase diagram of $TbNi_2B_2C$ is presented for $\mathbf{H}\|[110]$ and aspects of the similar H-T diagram for $\mathbf{H}\|[100]$ are discussed.

INTRODUCTION

The RNi_2B_2C series of compounds exhibits a wide variety of low-temperature (T) ground states ranging from superconductivity ($R=$ Lu, Sc, Y, Th), to superconductivity coexisting with magnetic order ($R=$ Tm, Er, Ho, and Dy), to magnetic order without superconductivity ($R=$ Gd).[1–7] These compounds crystallize in a layered crystal structure, which consists of the body-centered-tetragonal (bct) $ThCr_2Si_2$ structure with additional carbon atoms in each R layer.[8] Theoretically these compounds are expected to show electronically three-dimensional behavior and conventional BCS-type superconductivity.[9] Experimentally the $R=$ Tm, Er, Ho compounds undergo antiferromagnetic (AF) ordering in the superconducting state and display an interplay between the magnetic ordering and the superconductivity in resistivity measurements of polycrystalline samples.[2] Moreover, single crystals of each compound containing magnetic R atoms possess highly anisotropic normal-state magnetizations and also anisotropic and suppressed superconducting state properties, indicating the existence of significant interactions between the local magnetic moments and the superconducting electrons.[4–6] More recently the discovery of superconductivity at $T\approx 6$ K in single-crystal and polycrystalline $DyNi_2B_2C$ below the AF ordering temperature $T_N\approx 10.3$ K provided a rare example of superconductivity evolving out of an AF ground state.[7] $GdNi_2B_2C$, on the other hand, does not become superconducting for $T>2$ K,[2,10] even though it orders antiferromagnetically below 20 K.[10] Thus, with $GdNi_2B_2C$ and $DyNi_2B_2C$ as neighboring compounds, it is interesting to study the electronic and magnetic properties of single-crystal $TbNi_2B_2C$, which does not show any indication of superconductivity above 2 K in polycrystalline form.[2]

In this report, we present electronic transport and static magnetization (M) data of single-crystal $TbNi_2B_2C$. It is found that in addition to similarities with the $R=$ Dy, Tm, Er, and Ho compounds, a new feature, a weak ferromagnetic (WF) component, develops at $T\approx 9$ K, below $T_N=14.9$ K, and at low ($\leqslant 10$ kG) magnetic fields H. We will discuss the magnetic anisotropy in the normal state in terms of crystalline electric-field (CEF) effects and the possible origin of WF together with the in-plane magnetization anisotropy of $TbNi_2B_2C$. We will also discuss possible reasons for the lack of superconductivity in $TbNi_2B_2C$ based on the measured data.

EXPERIMENTAL DETAILS

Crystals of $TbNi_2B_2C$ were grown by the Ames Lab Ni_2B flux method.[5,11] This method yields plates of $TbNi_2B_2C$ with masses up to 300 mg with the crystallographic c-axis perpendicular to the plate surface. Powder x-ray-diffraction patterns of crushed single crystals show the crystals to be single phase. The three crystallographic axes ([100], [110], and [001]) were determined by Laue x-ray diffraction for the crystal which was used for magnetization measurements. $M(H,T)$ data were measured using a Quantum Design superconducting quantum interference device (SQUID) magnetometer. A Linear Research Inc. LR400 four-wire ac resistance bridge was used in conjunction with the T and H environmental control of the SQUID magnetometer to measure in-plane four-probe resistivity as a function of temperature.

RESULTS

Figure 1(a) shows $M(T)/H$ of single-crystal $TbNi_2B_2C$ for $\mathbf{H}\|[001]$ (M_{001}) and $\mathbf{H}\|[100]$ (M_{100}) with $H=10$ kG. Figure 1(b) shows inverse $M(T)/H$ data together with a calculated powder averaged curve $[(2M_{100}+M_{001})/3H]^{-1}$. The magnetization data are highly anisotropic, with a larger magnetization for $\mathbf{H}\|[100]$ than for $\mathbf{H}\|[001]$. The inverse $M(T)/H$ data for both field orientations in Fig. 1(b) show nearly linear behaviors above ≈ 100 K and deviate from the linear behaviors below 100 K for both directions of **H**. The inverse $M(T)/H$ of the powder average reveals a linear behavior for the whole temperature range above 15 K, concealing (averaging) the deviations observed for $\mathbf{H}\|\mathbf{c}$ and $\mathbf{H}\perp\mathbf{c}$

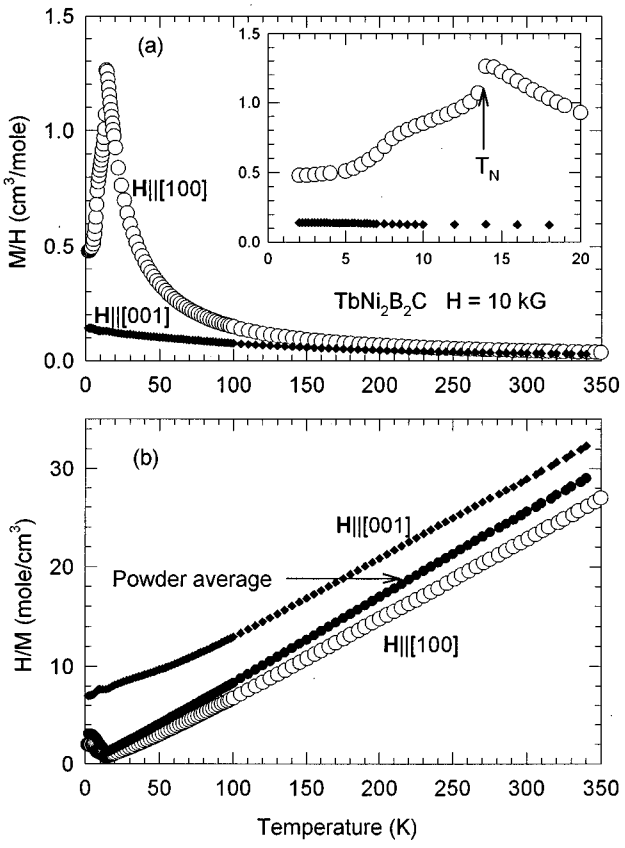

FIG. 1. (a) Anisotropic magnetization divided by applied magnetic field M/H versus temperature T for a $TbNi_2B_2C$ crystal for 2 K$\leqslant T\leqslant$350 K. Inset: Low-temperature data plotted on an expanded scale. (b) Inverse of M/H vs T for a $TbNi_2B_2C$ crystal, obtained from the data in (a). The closed circles represent $(M/H)^{-1}$ for a powder average (defined in text) of the M/H data for $\mathbf{H}\|[001]$ and $\mathbf{H}\|[100]$.

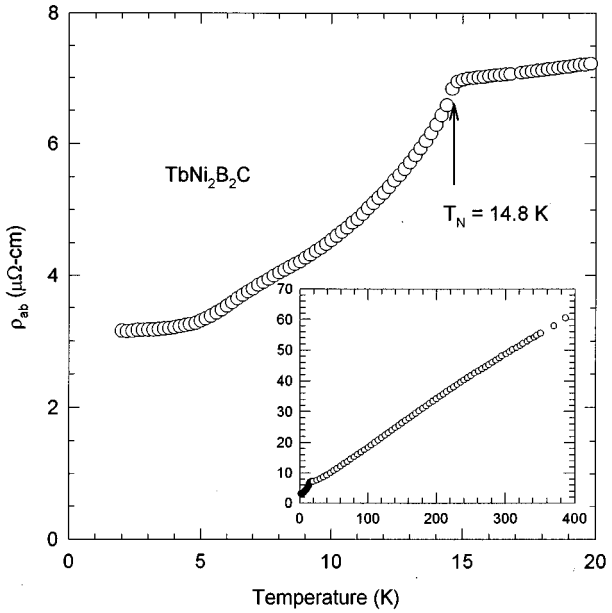

FIG. 2. Electrical resistivity in the ab plane (ρ_{ab}) versus temperature T for a $TbNi_2B_2C$ crystal for 2 K$\leqslant T\leqslant$20 K. Inset: ρ_{ab} versus T for 2 K$\leqslant T\leqslant$400 K.

below $\approx$100 K. Similar effects have already been seen in other RNi_2B_2C (R=Tm, Er, and Ho) single crystals.[4–6] The data above 100 K are fit to the Curie-Weiss law $M/H=C/(T-\theta)$, where the Curie constant $C=N\mu_{\rm eff}^2/3k_B$ and N is the number of Tb^{+3} ions. The effective magnetic moment $\mu_{\rm eff}$ of the Tb^{+3} ion is found to be $(9.9\pm0.1)\mu_B$, $(9.7\pm0.1)\mu_B$, and $(9.8\pm0.1)\mu_B$ for $\mathbf{H}\|[001]$, $\mathbf{H}\|[100]$, and the powder average, respectively. These values are in good agreement with the theoretical value $\mu_{\rm eff}=9.72\mu_B$ for the Hund's rule ground state of the isolated Tb^{+3} ion. The Weiss temperatures are found to be $\theta_{100}=(16\pm1)$ K, $\theta_{001}=(-60\pm1)$ K, and $\theta_{\rm avg}=(0\pm1)$ K for $\mathbf{H}\|[100]$, $\mathbf{H}\|[001]$, and the powder average, respectively. A phase transition near $T=14$ K is manifested as a sharp drop of the magnetization, as seen in Fig. 1(a) inset, consistent with antiferromagnetic ordering, which is also observed in other RNi_2B_2C (R= Er, Ho, Dy) crystals.[5–7] As will be shown below, field applied along the [100] direction suppresses T_N, and at $H=10$ kG T_N has dropped to 14 K from the low field value of 14.9 K. Another slope change in $M(T)$ is observed near 8 K [Fig. 1(a) inset].

In-plane resistivity (ρ_{ab}) data are plotted in Fig. 2 for 2 K $\leqslant T\leqslant$20 K and in the inset for 2 K$\leqslant T\leqslant$400 K. The residual resistivity ρ_{ab}(400 K)/ρ_{ab} (2 K) is $\approx$19. The average temperature coefficient of resistivity is $d\rho_{ab}/dT\approx0.15$ $\mu\Omega$ cm/K for 50 K$\leqslant T\leqslant$400 K which is comparable to that for single-crystal $ErNi_2B_2C$.[5] The overall ρ_{ab} vs T curve shows metallic behavior with slight negative curvature, which is very similar to the one in single-crystal $ErNi_2B_2C$, attributed to the short mean free path of conduction electrons due to the strong electron-phonon interaction.[5] A sharp increase in slope is seen upon cooling below the Néel temperature $T_N=14.8$ K, attributed to the loss of magnetic scattering. A small bump also occurs between 7 and 9 K. These two features occur at temperatures consistent with the temperatures at which there are features in the low-field magnetization measurement [Fig. 1(a) inset]. The drop of resistivity, $\Delta\rho_{ab}\equiv\rho_{ab}(15\ {\rm K})-\rho_{ab}$ (2 K), is near 3.8 $\mu\Omega$ cm. The $\Delta\rho_{ab}$, caused by the loss of magnetic scattering in the AF state, is given by[13]

$$\Delta\rho_{ab}=\frac{3\pi Nm^*}{2\hbar e^2\varepsilon_F}I^2{\rm DG}$$

where N is the number of magnetic moments, m^* is the effective mass of the conduction electrons, ε_F is the Fermi energy of the conduction electrons, DG $\equiv(g_J-1)^2J(J+1)$ is the de Gennes factor of the magnetic ions, g_J is the Landé factor, J is the angular momentum of the isolated R^{+3} ion, and I is the exchange interaction strength between the local magnetic moments and the conduction-electron spins. We estimate $I\approx5.2$ meV assuming that m^* is the free electron mass and the Fermi velocity is 2.1×10^5 m/sec.[9] This value is comparable with the value $I\approx13$ meV which is derived from the Abrikosov-Gor'kov theory of magnetic moments in superconductors.[2]

Figure 3 shows $M(T)$ data for several different magnetic fields from 1 to 40 kG applied along the [100] direction. The

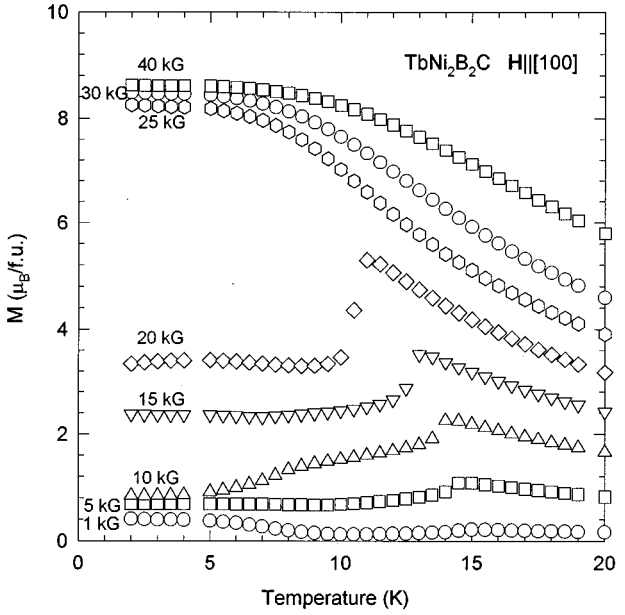

FIG. 3. Magnetization M versus temperature for a $TbNi_2B_2C$ crystal for various magnetic fields H with $\mathbf{H}\|[100]$.

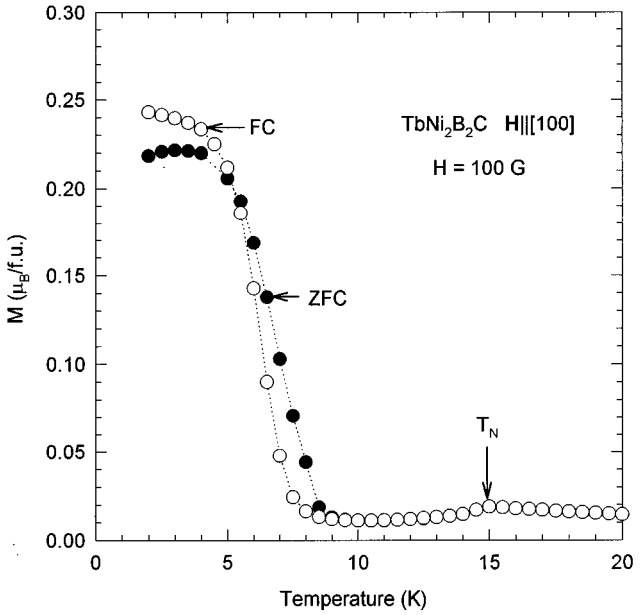

FIG. 4. Magnetization M versus temperature for a $TbNi_2B_2C$ crystal for applied magnetic field $H=100$ G with $\mathbf{H}\|[100]$. ZFC (full circles): data measured on warming after zero-field cooled, FC (open circles): data measured on cooling after field applied. The Néel temperature $T_N=14.8$ K is indicated.

T_N value, defined as the temperature of maximum $d(MT)/HdT$, decreases from 14.95 K at $H=1$ kG to 10.5 K at 20 kG, which is similar to $T_N(H)$ of single-crystal (Ho, Er)Ni_2B_2C.[5,6] Above 25 kG, the AF ordering disappears and the magnetization saturates below 5 K to between $8.2\mu_B$ and $8.7\mu_B$, depending on the applied field. These data indicate that a field-induced magnetic phase transition occurs for 20 kG$\leqslant H\leqslant$25 kG below 10 K. The phase transition observed in magnetization data in Fig. 1 and in the transport measurement in Fig. 2 near $T=8$ K is observed for $H=1$ kG as an increase of magnetization below 9 K, with $M\approx 0.4\mu_B$ at 2 K, indicating that a weak ferromagnetic (WF) component may develop out of the antiferromagnetic state for small applied magnetic fields. Above 10 kG, the feature near 8 K seems not to exist anymore indicating the possibility of a second magnetic phase transition.

In order to further understand the low-temperature and low-field region, we obtained $M(T)$ data with $H=100$ G and $M(H)$ data at $T=2$ K which are plotted in Fig. 4 and Fig. 5, respectively. In Fig. 4, in addition to the AF transition at $T_N\approx 15$ K, the WF component is seen to develop below ≈ 9 K and saturates below ≈ 4 K. The zero-field-cooled (ZFC) magnetization shows a lower saturation value at 2 K ($0.22\ \mu_B$) and higher onset temperature (≈ 9 K) of the weak ferromagnetism than the field-cooling (FC) magnetization ($0.25\mu_B$ and ≈ 8 K, respectively). Figure 5 shows a magnetic isotherm at 2 K. Whereas there is a hysteresis between the virgin curve 1 and the magnetization for field ramping down (curve 2), no noticeable hysteresis is found in the subsequent field sweeps indicated with arrows and numbers in Fig. 5. Extrapolating the higher field (500–1000 G) linear regions to zero field gives a saturated WF moment of $0.5\mu_B$.

To investigate the low-temperature magnetization anisotropy of the crystal, field-dependent magnetization measurements were performed at 2 K with the field applied in three different crystallographic directions, i.e., $\mathbf{H}\|[100]$, [110], and [001], and the results are plotted in Fig. 6. There are large anisotropies between all three orientations, i.e., not only between $\mathbf{H}\|[100]$ and $\mathbf{H}\|[001]$ but also within the *ab* plane, between $\mathbf{H}\|[100]$ and $\mathbf{H}\|[110]$. M_{001} is smaller than

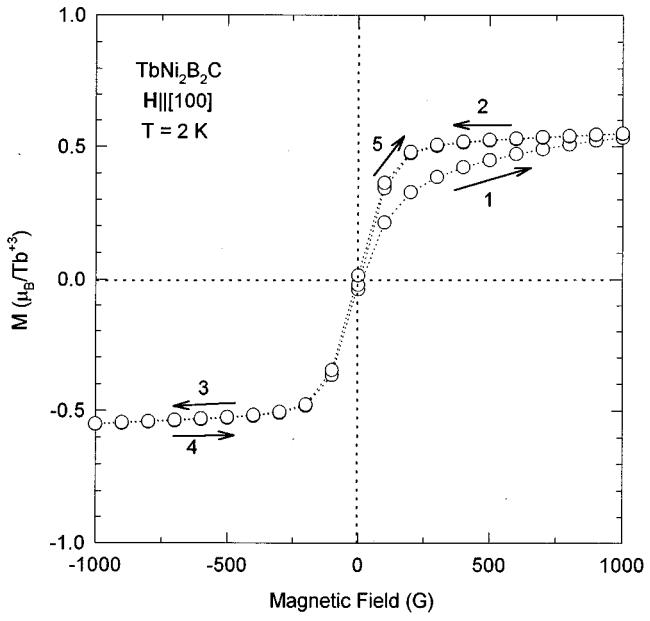

FIG. 5. Magnetization M versus applied magnetic field H for a $TbNi_2B_2C$ crystal for $\mathbf{H}\|[100]$ at $T=2$ K. The data are taken with the field history indicated with numbers and arrows, with number 1 being the virgin, zero-field-cooled, curve.

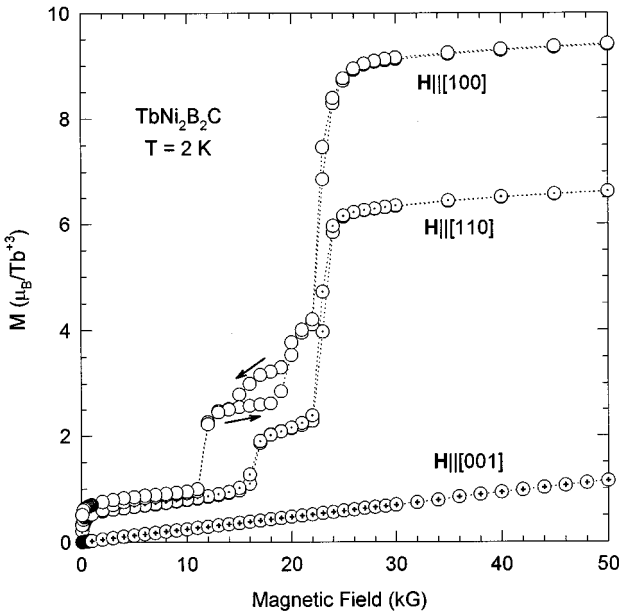

FIG. 6. Magnetization M versus applied magnetic field for a $TbNi_2B_2C$ crystal at $T=2$ K for $\mathbf{H}\|[100]$, $\mathbf{H}\|[110]$, and $\mathbf{H}\|[001]$.

both M_{100} and M_{110} and shows no field-induced magnetic transition below $H=50$ kG. It should be noted that the weak ferromagnetic moment, seen for both $\mathbf{H}\|[100]$ and $\mathbf{H}\|[110]$, does not appear for $\mathbf{H}\|[001]$. Within the basal plane, the anisotropy between M_{100} and M_{110} is most pronounced for H above the first metamagnetic transition at ≈ 11 kG. Whereas two metamagnetic transitions are found for $\mathbf{H}\|[110]$ near $H=16.5$ and 23 kG, there are three possible transitions evident for $\mathbf{H}\|[100]$. The significant hysteresis found for $\mathbf{H}\|[100]$ upon increasing and decreasing H, as shown by the arrows in Fig. 6, makes it difficult to resolve the nature or number of magnetic phases for H between 12 and 22 kG. The in-plane anisotropy of the saturated magnetic moment for $TbNi_2B_2C$ is qualitatively similar to that found for $HoNi_2B_2C$, which is interpreted in terms of anisotropy due to CEF interaction,[12] although in the case of $HoNi_2B_2C$ $M_{110}>M_{100}$ at 50 kG and 2 K. In the highest field (50 kG), the saturated paramagnetic moment of $\approx 6.6\mu_B$ for $\mathbf{H}\|[110]$ is significantly lower than the value of $\approx 9.5\mu_B$ for $\mathbf{H}\|[100]$. It should be noted that the $M_{100}\approx 9.5\mu_B$ at 2 K and 50 kG is significantly larger than the saturation moment of $9.0\mu_B$ for isolated Tb^{+3}. We speculate that the value of $M_{100}\approx 9.5\mu_B$ (larger by 5.5% than $9.0\mu_B$) comes from the ferromagnetic polarization of conduction-electron spins due to the exchange interaction between the local magnetic moments and conduction-electron spins. However, the estimated $\mu_{\rm eff}(\approx 9.8\mu_B)$ for the powder average is the same, within experimental error, as the theoretical $\mu_{\rm eff}$ value $(9.72\mu_B)$ of the Tb^{+3} Hund's rule ground state. More studies will be necessary to clarify the reason for this difference.

Figure 7 shows field-induced magnetic transitions below $H=50$ kG with $\mathbf{H}\|[110]$ at four different temperatures. At 2 K, there are two phase transitions near $H=16.5$ and 23 kG in addition to the weak ferromagnetic component in the low-field region as seen in Fig. 5. Thus, a metamagnetic state exists between 16.5 and 23 kG and a saturated paramagnetic

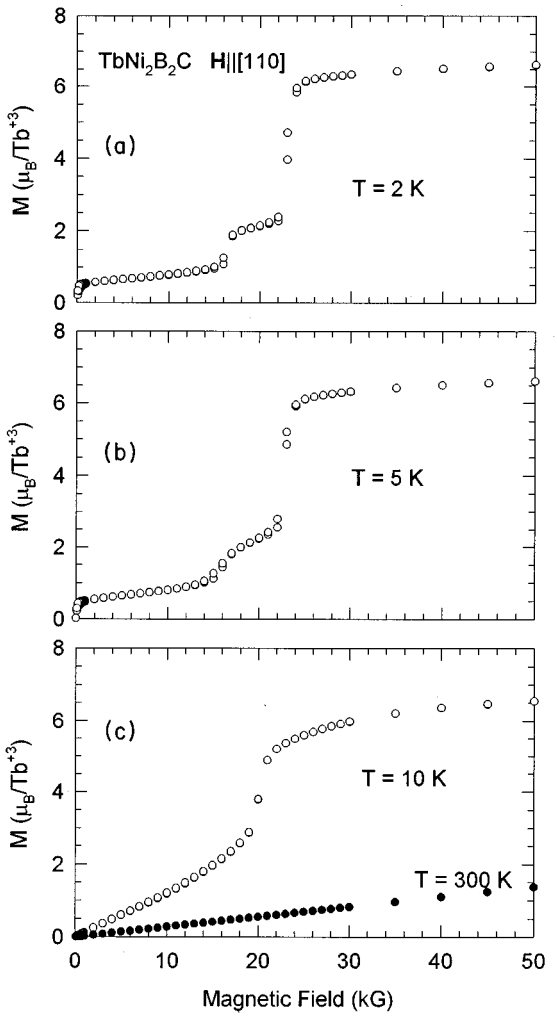

FIG. 7. Magnetization M versus applied magnetic field for a $TbNi_2B_2C$ crystal for $\mathbf{H}\|[110]$ at $T=$(a) 2 K, (b) 5 K, (c) 10 and 300 K.

state exists at higher fields. At $H=50$ kG the saturated magnetic moment of Tb^{+3} is $6.6\mu_B$, which is 73% of the theoretical maximum magnetization of $9\mu_B$. As the temperature increases, the first transition fades away and only one transition above $H=20$ kG remains at $T=10$ K and no WF component is detected at $T=10$ K. At $T=300$ K only a paramagnetic linear behavior of the magnetization versus field is seen.

DISCUSSION

Single crystals of RNi_2B_2C ($R=$ Dy, Ho, Er, and Tm) show large anisotropy in the normal-state magnetization that is attributed to crystalline electric-field (CEF) effects.[4–7] In a similar manner the magnetic anisotropy in $TbNi_2B_2C$ found here is also attributed to CEF effects. For the tetragonal point symmetry $(4/mmm)$ of an R ion in the RNi_2B_2C compounds, the CEF Hamiltonian can be written as[14]

$$\mathscr{H}_{\rm CEF}=B_2^0O_2^0+B_4^0O_4^0+B_4^4O_4^4+B_6^0O_6^0+B_6^4O_6^4, \qquad (1)$$

TABLE I. Values of the crystalline electric-field parameters B_2^0, and the parameters $\langle r^2\rangle$ (Ref. 17) and α_J (Ref. 16). All values are normalized to the values for Ho^{+3}. The easy axes from magnetization $M(H,T)$ and neutron-diffraction measurements are also listed.

	$\langle r^2\rangle$	α_J	B_2^0 (CEF)	B_2^0 (Exp)	Easy axis from $M(H,T)$	Easy axis from neut. diff.
Tb^{+3}	1.08	−4.55	4.914	3.9±0.1	$\mathbf{H}\perp\mathbf{c}$	
Dy^{+3}	1.04	−2.86	2.97	3.6±0.4 (Ref. 24)	$\mathbf{H}\perp\mathbf{c}$ (Ref. 7)	$\mathbf{H}\perp\mathbf{c}$ (Ref. 19)
Ho^{+3}	1	−1	1	1 (Ref. 13)	$\mathbf{H}\perp\mathbf{c}$ (Ref. 6)	$\mathbf{H}\perp\mathbf{c}$ (Refs. 20,21)
Er^{+3}	0.95	1.14	−1.08	−0.05±0.04 (Ref. 5)	$\mathbf{H}\perp\mathbf{c}$ for $T<150$ K $\mathbf{H}\parallel\mathbf{c}$ for $T>150$ K (Ref. 5)	$\mathbf{H}\perp\mathbf{c}$ (Refs. 22,23)
Tm^{+3}	0.91	4.5	−4.1	−2.9±0.5 (Ref. 4)	$\mathbf{H}\parallel\mathbf{c}$ (Ref. 4)	$\mathbf{H}\parallel\mathbf{c}$ (Ref. 24)

where the O_n^m are the Stevens equivalent operators and the B_n^m are the Stevens coefficients. The $B_2^0O_2^0$ term in $\mathscr{H}_{\rm CEF}$ is dominant in many cases and the field direction in which the susceptibility is largest is generally determined by the sign of B_2^0: *a* $B_2^0>0$ yields $M_{ab}>M_c$. Wang[15] and Boutron[16] showed that only the O_2^0 term among the terms in the CEF Hamiltonian contributes to the high-T Weiss temperatures in single crystals with R in tetragonal point symmetry. From the expansion of the susceptibility $\chi(T)$ as a power series in $1/T$, the value of B_2^0 can be calculated from the difference between θ_z and $\theta_{x,y}$ using the relation[16]

$$B_2^0=\frac{10}{3(2J-1)(2J+3)}(\theta_{x,y}-\theta_z), \tag{2}$$

where J is the angular momentum of the isolated ion, z is along the c axis, and x,y are, respectively, along the a and b axes of the tetragonal structure. Equation (2) is derived based on the assumption of uncoupled ions, i.e., no exchange interaction between rare-earth ions. By using the values of θ_z and $\theta_{x,y}$ found above from Fig. 1(b), B_2^0 is estimated to be (1.54±0.04) K, the sign of which is consistent with the observed sign of the magnetization anisotropy. The positive sign of B_2^0 is also consistent with the sign of B_2^0 for other $R\mathrm{Ni_2B_2C}$ compounds[4,5,12] and the theoretical expectation of the point-charge model of CEF.

In the point-charge model, B_2^0 can be written as

$$B_2^0=\langle r^2\rangle A_2^0\alpha_J, \tag{3}$$

where $\langle r^2\rangle$ is the mean-square radius of the $4f$ electrons, A_2^0 represents the electrostatic effects from the static charges of the lattice of neighboring ions, and α_J is the Stevens multiplicative factor. Assuming that A_2^0 has a sign independent of particular rare-earth element among an isostructural series of compounds, and since the radial integral is positive by definition, the sign of B_2^0 depends only on the sign of α_J, which is negative for Tb^{+3}.[17] This gives nice agreement with the observed sign of B_2^0 of $\mathrm{TbNi_2B_2C}$, assuming A_2^0 is negative, as shown in Table I. The values of $\langle r^2\rangle$ normalized to the value of $\langle r^2\rangle$ for Ho^{+3} (Ref. 18), and the α_J values, normalized to the α_J for Ho^{+3}, are also listed. Assuming that A_2^0 is constant within the $R\mathrm{Ni_2B_2C}$ series, the theoretical and experimental estimations of B_2^0, both normalized to the Ho^{+3} values, are also presented for comparison. Within the experimental error the point-charge CEF model predicts the sign of B_2^0 correctly, according to the easy axis as observed in magnetization[4–7] and neutron-diffraction[19–24] measurements. However, the normalized experimental magnitudes of B_2^0 do not seem to be in such good agreement with the theoretical predictions. This discrepancy may come from the assumptions that A_2^0 is constant through the $R\mathrm{Ni_2B_2C}$ series and that the point-charge model applies, or may be due to the isolated ion assumption we have made in using Eq. (2).

For 8 K $\leqslant T\leqslant$ 14.9 K, $\mathrm{TbNi_2B_2C}$ is ordered antiferromagnetically in low applied magnetic field. The magnetization data shown in Fig. 1 are similar to those for the $R\mathrm{Ni_2B_2C}$ ($R=$ Er, Ho, Dy) (Refs. 5 and 7) compounds below their magnetic ordering temperatures. However, as has been found in neutron-diffraction studies,[19–23] the $R=$ Er, Ho, and Dy compounds each have different magnetic structures at low temperatures. Other than our inference that the ordered moment will be oriented near to or in the basal plane of the tetragonal structure, the details of the magnetic structure of $\mathrm{TbNi_2B_2C}$ must await the results of neutron-diffraction or magnetic x-ray-diffraction studies. The data shown in Figs. 3–5 indicate the existence of magnetic order with a weak ferromagnetic (WF) component below $T\approx 8$ K at low fields. [See noted added.] The weak ferromagnetism seems to be an intrinsic feature of the $\mathrm{TbNi_2B_2C}$ ground state. The anisotropy of the WF state shown in Fig. 6 rules out the possibility of the WF coming from a polycrystalline impurity phase, and the feature being seen in both the magnetization and the electrical resistivity data near 8 K is consistent with a bulk WF transition. This weak ferromagnetism in low field is, so far, peculiar to $\mathrm{TbNi_2B_2C}$ among the $R\mathrm{Ni_2B_2C}$ ($R=$ Gd–Tm) series and makes this compound of special interest.

Dzialoshinskii[25] showed that a WF state is possible in the space group D_{4h}^{14} ($P4_2/mnm$) of $\mathrm{NiF_2}$, where the Ni has the same point symmetry that Tb^{+3} has in $\mathrm{TbNi_2B_2C}$. By minimizing the thermodynamic potential consistent with the crystal symmetry, he suggests five possible antiferromagnetic states, out of which four states can show a canted magnetic moment. Two of these four states have the AF components of the ordered moments $\perp_c$, and two $\parallel\mathbf{c}$. In the former case, the canted moment can be either $\parallel[100]$ or $\parallel[110]$. From Fig. 1, the Tb^{+3} moments have an easy (ab) plane. Thus, two different canted AF magnetic states can be stabilized in $\mathrm{TbNi_2B_2C}$, corresponding to the AF components of the staggered moments lying along [100] or along [110]. It should be

noted that the easy magnetization axis within the basal plane is along [100] in $TbNi_2B_2C$ (see Fig. 6) rather than [110] as in (Ho,Dy)Ni_2B_2C,[12,26] which show no WF transition. We therefore speculate that the easy magnetization direction of [100] in $TbNi_2B_2C$ may have a close relation with the occurrence of the WF state. Moriya[27,28] developed the microscopic theory of weak ferromagnetism based on Dzialoshinskii's phenomenological model. He showed that the CEF effects together with spin-orbit coupling lead to a WF moment in NiF_2 ($T_N \approx 7.3$ K),[27] and that the antisymmetric anisotropic superexchange interaction (the so-called Dzialoshinskii-Moriya interaction) appears to be the origin of weak ferromagnetism in α-Fe_2O_3 ($T_N \approx 950$ K).[28] We speculate that the former mechanism is likely to be responsible for the observed weak ferromagnetism in $TbNi_2B_2C$ because the later mechanism is likely to be more important for antiferromagnetic materials with high Néel temperature, for then the exchange interaction is large.[28]

Recently the onset of superconductivity in single-crystal $DyNi_2B_2C$ was found[7] ($T_c = 6.2$ K) below the long-range AF ordering temperature ($T_N = 10.3$ K). Given that $T_N > T_c$ in $DyNi_2B_2C$, the possibility of superconductivity in $TbNi_2B_2C$ ($T_N = 14.9$ K) should be examined. In fact, if one extrapolates the line for T_c (DG) between the Lu and Dy members to the DG factor of Tb^{+3}, one obtains the predicted $T_c \approx 1.2$ K for $TbNi_2B_2C$ (which is below the low-temperature limit of 2 K of the measurements of $TbNi_2B_2C$ up to now). On the other hand, it is worthwhile to notice that the saturated magnetization at high magnetic field and low temperature is higher than the theoretical maximum magnetization (see Fig. 6) whereas the single crystal (Dy,Ho,Er)Ni_2B_2C shows a saturated magnetization close to or slightly lower than the theoretical maximum magnetization.[5,12,26] This may be due to different sign of I from that found for (Er,Ho,Dy)Ni_2B_2C, which may be relevant to determining T_c. In addition, the WF moments developing below ≈ 8 K at zero magnetic field will be detrimental to superconductivity. The calculated $4\pi M \approx 900$ G from the WF moments is comparable with the thermodynamic critical fields (H_c) of the superconducting RNi_2B_2C compounds. For example, the H_c of YNi_2B_2C (Ref. 29) single crystal was shown to be near 2.5 kG at 2K and the H_c of $ErNi_2B_2C$ (Ref. 5) single crystal can be estimated to be near 1.2 kG from the relation $H_c = H_{c2}/\sqrt{2}\kappa$ here H_{c2} is the upper critical field and κ is the Ginzburg-Landau parameter.

It is worthwhile to mention here that while single-crystal $ErNi_2B_2C$ exhibits field-induced magnetic transitions at $T = 2$ K similar to the two transitions in $TbNi_2B_2C$ near $H = 16.5$ and 22 kG in Fig. 7, two additional weak field-induced transitions at $T = 2$ K for $H \approx 1$ and 7 kG of unknown origin were reported in our previous paper (Ref. 5). With the present clear evidence of a WF state in $TbNi_2B_2C$, we suspect that the transition near $H \approx 1$ kG in $ErNi_2B_2C$ may be related to a WF state. In that case the WF magnetization adds to, and is masked by, that of the superconducting diamagnetism, so that it is difficult to identify the WF state from magnetization measurements. Thus it will be of great interest to further investigate the coexistence of a possible WF state with superconductivity in $ErNi_2B_2C$.

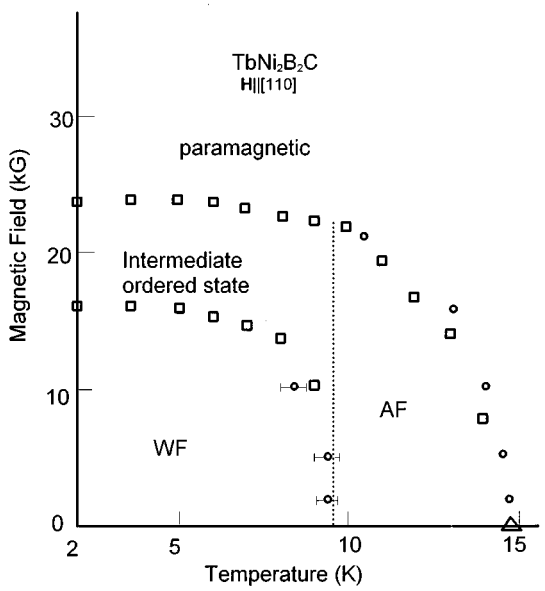

FIG. 8. Magnetic field versus temperature magnetic phase diagram for a $TbNi_2B_2C$ crystal. □: data taken from M vs H isotherms for $\mathbf{H}\|[110]$, ○: data taken from M vs T measurements for $\mathbf{H}\|[110]$, and △: data taken from ρ_{ab} vs T. Abbreviations: AF (antiferromagnetic); WF (weakly ferromagnetic). The nature of the ''intermediate ordered state'' is not known.

Based upon $M(T)$ data as in Fig. 3 and $M(H)$ isotherms such as in Figs. 6 and 7, the H-T magnetic phase diagram of $TbNi_2B_2C$ was studied and the results for $\mathbf{H}\|[110]$ are plotted in Fig. 8. The squares are the magnetic transition fields defined as the fields of maximum slope of M versus H isotherm data. The data similarly derived from M vs T measurements at fixed H (circles) agree well with the data from the M vs H isotherms in the overlapping region. In zero field, the T_N from ρ_{ab} vs T in Fig. 2 is also plotted as a triangle. The upper phase boundary (which starts at $T_N = 14.9$ K in low field and saturates at 24 kG for temperatures below 5 K) represents the boundary between paramagnetism (higher temperature and fields) and magnetic order (lower temperatures and fields). The inner phase boundary divides the weakly ferromagnetic state (the lowest temperature and field state) from an unknown type of magnetically ordered state labeled ''intermediate ordered state.'' This intermediate region of the phase digram may contain more than one type of magnetic order. Temperature and field-dependent neutron diffraction will help refine our understanding of this region.

In addition to the H-T phase digram shown in Fig. 8 for $\mathbf{H}\|[110]$, we have some qualitative understanding of the features of the H-T phase diagram for $\mathbf{H}\|[100]$. For $\mathbf{H}\|[100]$ the outer phase boundary is identical with that for $\mathbf{H}\|[110]$, to within our precision. The inner phase boundary is more difficult to determine due to the hysteresis in $M(H)$ seen in Fig. 6. If we focus on the nonhysteretic features, the lower phase boundary that delineates the WF region saturates at a lower field ($H \approx 12$ kG instead of $H \approx 16$ kG for $\mathbf{H}\|[110]$). On the other hand, there may be an extra phase boundary between $H \approx 12$ and $H \approx 24$ kG. Due to the

hysteresis in the $M(H)$ isotherms, details associated with this intermediate H-T region will require further measurements.

CONCLUSION

We have performed extensive magnetization measurements on single-crystal $TbNi_2B_2C$ as well as measurements of $\rho_{ab}(T)$. We find the onset of antiferromagnetic order at $T_N = 14.9$ K in low fields ($H \leqslant 100$ G), followed by the onset of a weakly ferromagnetic phase for $T \leqslant 8$ K. No superconductivity is detected in either magnetization or resistivity measurements for $T > 2$ K. This lack of superconductivity may be due to the enhanced pairbreaking of the Tb^{+3} ion as predicted by de Gennes scaling, and/or it may be associated with the weak ferromagnetism present below 8 K.

$TbNi_2B_2C$ has a highly anisotropic magnetization both above and below $T_N \approx 14.9$ K with M_{001} being lower than M_{100} and M_{110} at all measured temperatures and fields. Below 14.9 K there is an anisotropy between M_{100} and M_{110}, particularly for H above the critical field(s) associated with the transition from the low-field ordered state to the intermediate-field ordered state. The high-field saturated moment is larger for $\mathbf{H} \| [100] (\approx 9.5 \mu_B)$ than for $\mathbf{H} \| [110] (\approx 6.6 \mu_B)$. This anisotropy is opposite to that found for $HoNi_2B_2C$ and may be related to the existence of the WF phase.

Note added: Temperature-dependent neutron-scattering measurements have recently been completed on $TbNi_2B_2C$ single crystals in zero applied magnetic field.[30] These measurements show that the Tb sublattice is disordered for temperatures above 15 K, ordered in an incommensurate, modulated antiferromagnetic structure for temperatures below 15 K, and develops a ferromagnetic component for temperatures below 8 K.

ACKNOWLEDGMENTS

We thank C. Detlefts for orienting the $TbNi_2B_2C$ crystal used for the $M(T,H)$ measurements. Ames Laboratory is operated for the U.S. Department of Energy by Iowa State University under Contract No. W-7405-Eng-82. This work was supported by the Director for Energy Research, Office of Basic Energy Sciences.

[1] R. Nagarajan, Chandan Mazumdar, Zakir Hossain, S. K. Dhar, K. V. Gopalakrishnan, L. C. Gupta, C. Godart, B. D. Padalia, and R. Vijayaraghavan, Phys. Rev. Lett. **72**, 274 (1994).

[2] R. J. Cava, H. Takagi, H. W. Zandbergen, J. J. Krajewski, W. F. Peck, Jr., T. Siegrist, B. Batlogg, R. B. van Dover, R. J. Felder, K. Mizuhashi, J. O. Lee, H. Eisaki, and S. Uchida, Nature (London) **367**, 252 (1994); H. Eisaki, H. Takagi, R. J. Cava, K. Mizuhashi, J. O. Lee, B. Batlogg, J. J. Krajewski, W. F. Peck, Jr., and S. Uchida, Phys. Rev. B **50**, 647 (1994).

[3] H. C. Ku, C. C. Lai, Y. B. You, J. H. Shieh, and W. Y. Guan, Phys. Rev. B **50**, 351 (1994); J. L. Sarrao, M. C. de Andrade, J. Hermann, S.H. Han, Z. Fisk, M. B. Maple, and R. J. Cava, Physica C **229**, 65 (1994); C. C. Lai, M. S. Lin, Y. B. You, and H. C. Ku, Phys. Rev. B **51**, 420 (1995).

[4] B. K. Cho, Ming Xu, P. C. Canfield, L. L. Miller, and D. C. Johnston, Phys. Rev. B **52**, 3676 (1995).

[5] B. K. Cho, P. C. Canfield, L. L. Miller, D. C. Johnston, W. P. Beyermann, and A. Yatskar, Phys. Rev. B **52**, 3684 (1995).

[6] P. C. Canfield, B. K. Cho, D. C. Johnston, D. K. Finnemore, and M. F. Hundley, Physica C **230**, 397 (1994); K. D. D. Rathnayaka, D. G. Naugle, B. K. Cho, and P. C. Canfield, Phys. Rev. B **53**, 5688 (1996).

[7] B. K. Cho, P. C. Canfield, and D. C. Johnston, Phys. Rev. B **52**, R3844 (1995); M. S. Lin, J. H. Shieh, Y. B. You, Y. Y. Hsu, J. W. Chen, S. H. Lin, Y. D. Yao, Y. Y. Chen, J. C. Ho, and H. C. Ku, Physica C **249**, 403 (1995).

[8] T. Siegrist, H. W. Zandbergen, R. J. Cava, J. J. Krajewski, and W. F. Peck, Jr., Nature (London) **367**, 254 (1994).

[9] Warren E. Pickett and David J. Singh, Phys. Rev. Lett. **23**, 3702 (1994); L. F. Mattheiss, Phys. Rev. B **49**, 13 279 (1994).

[10] P. C. Canfield, B. K. Cho, and K. W. Dennis, Physica B **215**, 337 (1995).

[11] M. Xu, P. C. Canfield, J. E. Ostenson, D. K. Finnemore, B. K. Cho, Z. R. Wang, and D. C. Johnston, Physica C **227**, 321 (1994).

[12] B. K. Cho, B. N. Harmon, D. C. Johnston, and P. C. Canfield, Phys. Rev. B **53**, 2217 (1996).

[13] E. Gratz and M. J. Zuckermann, in *Handbook on the Physics and Chemistry of Rare Earths*, Vol. 5, edited by K. A. Gschneider, Jr. and L. Eying (North-Holland, Amsterdam, 1982), p. 117.

[14] John L. Prather, Natl. Bur. Stand. (U.S.) Monograph No. 19 (U.S. G.P.O., Washington, D.C., 1961).

[15] Yang-Li Wang, Phys. Lett. **35A**, 383 (1971).

[16] Pierre Boutron, Phys. Rev. B **7**, 3226 (1973).

[17] M. T. Hutchings, in *Solid State Physics: Advances in Research and Applications*, edited by Frederick Seitz and David Turnbull (Academic, New York, 1964), Vol. 16, p. 227.

[18] A. J. Freeman and R. E. Watson, Phys. Rev. **127**, 2085 (1962).

[19] P. Dervenagas, J. Zarestky, C. Stassis, A. I. Goldman, P. C. Canfield, and B. K. Cho, Physica B **212**, 1 (1995).

[20] A. I. Goldman, C. Stassis, P. C. Canfield, J. Zarestky, P. Dervenagas, B. K. Cho, D. C. Johnston, and B. Sternleib, Phys. Rev. B **50**, 9668 (1994).

[21] T. E. Grigereit, J. W. Lynn, Q. Huang, A. Santoro, R. J. Cava, J. J. Krajewski, and W. F. Peck, Jr., Phys. Rev. Lett. **73**, 2756 (1994).

[22] J. Zarestky, C. Stassis, A. I. Goldman, P. C. Canfield, P. Dervenagas, B. K. Cho, and D. C. Johnston, Phys. Rev. B **51**, 678 (1995).

[23] S. K. Sinha, J. W. Lynn, T. E. Grigereit, Z. Hossain, L. C. Gupta, and R. Nagarajan, Phys. Rev. B **51**, 681 (1995).

[24] C. Stassis (private communication).

[25] I. E. Dzialoshinskii, Sov. Phys. JETP **6**, 1120 (1958).

[26] B. K. Cho and P. C. Canfield (unpublished).

[27] Tôru Moriya, Phys. Rev. **117**, 635 (1960).

[28] Tôru Moriya, Phys. Rev. **120**, 91 (1960).

[29] R. Movshovich, M. F. Hundley, J. D. Thompson, P. C. Canfield, B. K. Cho, and A. V. Chubukov, Physica C **227**, 381 (1994).

[30] P. Dervenagas, J. Zarestky, C. Stassis, A. I. Goldman, P. C. Canfield, and B. K. Cho, following paper, Phys. Rev. B **53**, 8506 (1996).